CHARACTERISATION OF FOAM PROPERTIES USING IMAGE ANALYSIS

DIPAK K. SARKER[1], DOMINIQUE BERTRAND[2,3], YOUNÈS CHTIOUI[2]
and YVES POPINEAU[1]

Institut National de la Recherche Agronomique
[1]*Unité de Biochimie et Technologie de Protéines*
[2]*Unité Phytec*
rue de la Géraudière
BP- 71627, 44316 Nantes cedex 03, France

ABSTRACT

The physical properties of a series of model protein, surfactant and protein/surfactant foams were enumerated and investigated using foam conductivity, surface tension, preliminary surface rheology and bulk viscosity measurements. Images of various predetermined stages in the evolution of foam samples were obtained. Foam images were recorded, digitised and analysed using mathematical analysis of image texture. A textural appreciation was achieved by counting bubbles in selected images at key points during the evolution of the foam. Statistical treatment allowed delineation of real and mathematical artefacts generated in textural descriptions of foams. A principal component analysis parameter was identified, which not only corresponded with bubble size but also described bubble shape and occurrence in the texture. Analysis of the data showed correlations between sample images and changes in the structure and the composition of the adsorbed interfacial layer, highlighted using physical measurements.

INTRODUCTION

A broad range of food products exist in the form of dispersions. These dispersions most frequently take the form of either simple, or more usually, complex

foam and emulsion systems. Although relatively simple in appearance the underly-
ing science of foam formation, drainage, and stability is extremely complex
(Dickinson and Stainsby 1982; Germick *et al.* 1994). Thus, more conventional
techniques (e.g. conductimetry, surface rheology) used to identify the properties
of food dispersions can provide a means by which the physical and perceived
qualities of the food can be assessed. One limitation with foam-like dispersions
is that the conventional measurements are seldom undertaken on an intact foam
and therefore are not as representative as is often assumed.

An alternative and complementary approach is to consider that changes in the
images of the dispersion as a function of time, for example a foam, represent
differences in the structure. Rather than in terms of charting the 3-dimensional
(3-D) physical properties it is possible that much of the sample information is
contained in 2-dimensions (2-D), with the image composed of regular units (i.e.
pixels) of variable intensity. This visual texture, hereafter referred to as texture,
contains much of the information of the original sample but in a form that can
be evaluated in an easier fashion than in the parent foam. Under standardised
conditions it is possible to evaluate the image to isolate particular properties of
the original foam. Work performed previously with 2-D images of natural land-
scapes and artificially created images (Galloway 1975; Lohmann 1995), powders
and bread (Bertrand *et al.* 1991, 1992), biological samples (Chu *et al.* 1990) and
foams (Guillerme *et al.* 1993; Fains *et al.* 1997) has shown that textural analysis
can be extremely discriminating with respect to images.

Pattern recognition has become an increasingly complex area of research over
the past two decades. At present an enormous variety of techniques exist, all of
which can be used to analyse images (Conners 1980; Haralick 1979). Among
all the mathematical techniques used for characterising the textural appearance
of foams the grey level run length (GLRL) method is known to be efficient and
has been used in several studies. As this method is relatively simple to compute
and analyse it was chosen in the present study. We have used grey level run length
matrices (GLRLM; grey value distribution of run length matrices) to treat the
images of foams used in this study.

The aim of this study is to use both physical measurements and mathematical
treatment of digitised images to describe more fully the properties of foams. In
using highly standardised air-water foams prepared with purified surfactants (pro-
teins and emulsifiers) thus creating model systems for study, we have been able
to evaluate the characteristics of the foams. In addition, by using both statistical
manipulation and conventional measurements we hope to be able to evaluate the
relative importance of the mathematical treatment.

MATERIALS AND METHODS

Preparation of Samples

Protein samples, bovine serum albumin (BSA; A-9647), β-casein (C-6905) and ovotransferrin (conalbumin; C-1130) were obtained from the Sigma Chemical Co., USA. The purified nonionic food emulsifier, polyoxyethylene (20) sorbitan monolaurate (Tween 20) was purchased as a 10% solution from Pierce, USA (No. 28320). All samples were prepared in 0.1 mol dm^{-3} (M) sodium phosphate buffer using surface chemically pure water (surface tension 72.8 mNm^{-1}) adjusted to pH 7.0. The concentration of protein solutions was determined spectrophotometrically at 280 nm using absorbance coefficients of 0.66, 0.44 and 0.989 mg. mL^{-1}.cm^{-1} for BSA, β-casein and ovotransferrin, respectively. Foam solution sample details and nomenclature are presented in Table 1.

Physical Measurements

Conductivity Apparatus. The apparatus (Fig. 1) consists of a 22.5 cm glass column with internal and external diameters of 2 and 3 cm, respectively. Test solution (8 mL) was placed in the dry column. A sintered metal frit (2 μm average pore size) at the base of the glass column rests within a perspex body which contains the enclosed sparging chamber. Pure nitrogen gas at a pressure of 1 bar and a flow rate of 15 mL min^{-1} was passed into the sparging chamber and forced under pressure through the test liquid in the glass column creating the foam body. The conductivity during the test, volume of foam and air incorporated are recorded by the IBM-Compatible microcomputer and linear camera (Schmersal OM-1024 with Cosmicar 25 mm television lens). The height of the column of foam (35 mL) and the sparging of the test solution are all controlled by the governing software (Fains *et al.* 1997; Loisel *et al.* 1993) in response to the linear camera.

Conductivity measurements as a function of time (C_t) and with reference to the conductivity of the buffered test solution (C_{init}) were used to calculate the volume of liquid entrained in the foam (V_L) according to Loisel *et al.* (1993).

$$V_L = V_{init}[1 - (C_t/C_{init})] \tag{1}$$

where V_{init} is the volume of sample solution (8 mL) introduced into the apparatus.

This relative volume of liquid entrained in the foam (V_L) was then used as an indication of foamability (foam forming ability) and foam stability. Here the foamability is defined as the initial foam density, immediately after sparging (D_0) and the foam stability (D_{660}) defined as the foam density 11 min after commencement of the experiment. These 'relative' expressions of foam density are simply calculated as the volume of liquid in the foam (V_L) at a specified time divided

TABLE 1.
SAMPLE DETAILS OF FOAM IMAGES

LABEL	Composition	Specific details
CA, CB, CC	42 μM β-casein	-
CAX, CBX, CCX	42 μM β-casein + 6 μM Tween 20	molar ratio, $R=0.15$*
OA, OB, OC	26 μM ovotransferrin	-
OAX, OBX, OCX	26 μM ovotransferrin + 9 μM Tween 20	molar ratio, $R=0.35$*
BA, BB, BC	22 μM bovine serum albumin	-
TA, TB, TC	500 μM Tween 20	-
TAV, TBV, TCV	500 μM Tween 20 in 0.25 M buffered sucrose	increased bulk viscosity

* - as part of calibration studies (not shown), these ratios were determined to exist in the initial part (corresponding to an increased foam drainage rate) of the foam stability curves, as a function of Tween 20 concentration

by the volume of nitrogen incorporated in constant volume of foam (35 mL). The volume of liquid entrained in the foam is calculated from the change in conductivity of the liquid at the base of the foam between the two large electrodes during foaming. Since the conductivity of the buffer (which changed linearly in this range with ionic strength) under the constant temperature conditions of the room (20 ± 1C) remained constant or with negligible change, the conductivity (approx. 2 mS.cm^{-1}) was a direct measure of the quantity of liquid entrained in the foam.

Surface Tension. Dynamic and static measurements of surface tension of 25 mL diluted protein and surfactant solutions were performed using a Krüss digital tensiometer K10T (Germany) at 20 ± 1C in a vapour saturated environment using a platinum-iridium Wilhelmy plate. The tensiometer was linked to an IBM-compatible PC. Data were acquired with a software package (written in-house) which also enabled collection of surface tension data over variable time periods.

Kinematic Viscometry. Newtonian sample solutions of 2 mL (identical in composition to those used for foaming experiments) were prefiltered using Whatman GFD 2.7 μm pore size filtration units. Measurements were performed using a Schott-Geräte 51810/I Ostwald micro-viscometer (Germany) at 20 ± 0.5C in an accurately thermostated water bath after a thermal equilibration period of 10 min. The flow time of the sample solution between two graduations is proportional to the kinematic viscosity.

Surface Shear Rheology Measurements. A 6 cm diameter aluminium 'sharp-edged' inverted cup-shaped measuring body (built in-house) located at the interface, similar to the measuring body used by Krägel et al. (1994) was connected to a Carri-Med CS Rheometer (England) to determine relative values of the sur-
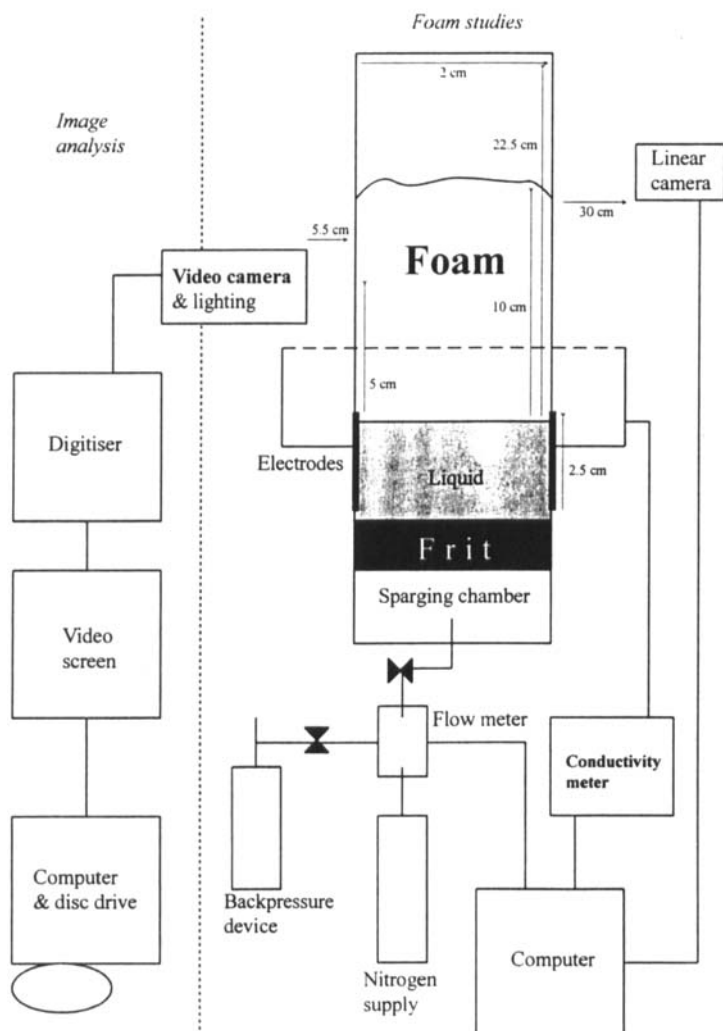
FIG. 1. SCHEMATIC REPRESENTATION (NOT DRAWN TO SCALE) OF THE
FOAMING AND IMAGE ACQUISITION EQUIPMENT
The figure is divided into two parts showing the conductivity (foam study) apparatus
and the image analysis units.

face shear rigidity. The relative surface shear rigidity is defined here as the
measured torque, applied to sustain an angular velocity of the measuring body
of 0.1 radians s^{-1}. The apparatus gives limited but discernible information on
the gross properties of the adsorbed interfacial layer. All measurements were per-
formed in a firmly secured 7 cm diameter glass vessel with 35 mL test solution

at 20C in a vapour saturated atmosphere after an equilibration period of 40 min. The concentrations of β-casein, bovine serum albumin, ovotransferrin and Tween 20 used in determinations were 42, 22, 26 and 500 μM, respectively.

Image Acquisition and Analysis

Image Capture. Foams formed in the conductivity apparatus were illuminated with an 11W white light source placed at an angled position below the foam column so that the foam sample was illuminated maximally. A Sony CCD video camera (Japan) fitted with a 28–70 mm f/3.5–f/4.5D Nikkor FAF objective lens (Nikon, Japan) located at a position 5 cm above the base of the foam sample and 5.5 cm from the outer wall of the foaming vessel was used to capture foam images (Fig. 1). This position corresponds to a portion of the bubbles in the foam placed at the glass surface but in the exact centre of the exterior of the foam body. Images were collected on a PCSCOPE system (i2S, France) composed of an IBM-compatible PC equipped with electronic card (Sony camera adapter CAM D5CL, Japan) for digitisation of the image. Monochrome images acquired represented an area of 5 mm × 5 mm. Images were digitised in the form of pixel arrays having dimensions of 512 rows by 512 columns. Individual pixel intensities scaled in integer values from 0 (white) to 255 (black) for a given image.

For each repetition, 11 images were acquired separated by a period of 120 s, corresponding to a 20 min total run time. Individual sample solution image repetitions were recorded in a random manner using identical solutions (and performed in triplicate). In the case where a collapsed foam series of images were recorded these were omitted from further treatment because no bubbles were present or residual portions of the foam adhered to the vessel wall. Further treatment of such images would be misleading. Two hundred and eighteen images were captured in total, corresponding to the 7 samples multiplied by the 3 repetitions less the collapsed foam images (13). The images were stored on a Maxell CD-R 680Mb compact disc for mathematical treatment.

Simple Bubble Counting Technique. A very straightforward technique where dissecting lines were placed in the centre of each image in horizontal and vertical directions when the image was displayed on a computer screen. These lines temporarily placed on the image, were used to enumerate the number of bubbles in a horizontal (H_c) or vertical direction (V_c) within the image that corresponded to a 5 mm × 5 mm area of the foam at the vessel wall (Fig. 2). The foam images had the same orientation as when captured and stored for texture analysis. The technique was performed by visual counting of the number of bubbles, full or part, which were traversed by each of the lines. The technique is of use in describing the fine structure or coarseness of the foam but does not give an indication of bubble morphology.

Vc=7

Hc=7

Digitised image   Bubble count [(Hc +Vc)/2] =7
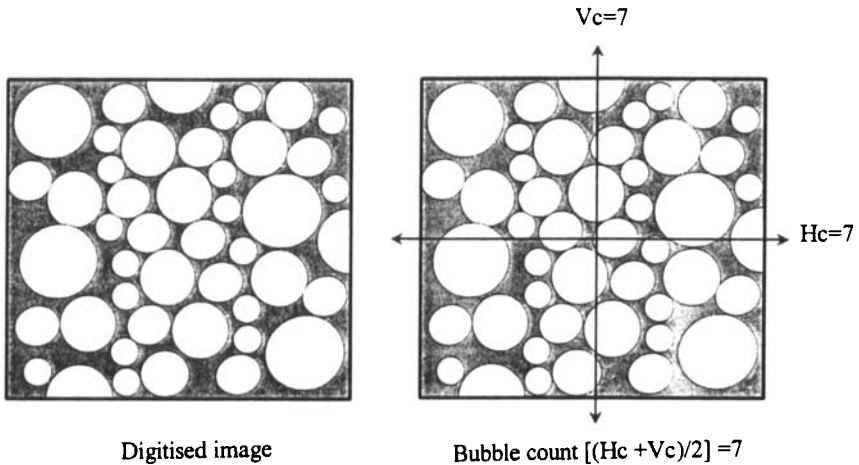
FIG. 2. SCHEMATIC REPRESENTATION OF THE SIMPLE BUBBLE COUNTING
TECHNIQUE PERFORMED ON DIGITISED FOAM IMAGES

Grey Level Run Length Matrices. A grey level run length is a set or series
of consecutive collinear picture points with a defined intensity (Galloway 1975;
Haralick 1979). This technique works by extracting a matrix $(i, j | \theta)$ from a digitis-
ed image, where i is the maximum length of the body (i.e. a body of 512×512
pixels gives a value of i of 512) and where j is the total possible number of grey
levels (intensities) in the image which is 256 (i.e. 0 to 255). The matrix is created
by selecting the angle over which the examination of the matrix will take place
(θ). This is customarily $0°$ or $90°$. The number of occurrences of the intensity
elements 0–255 that occur in the image matrix with the full range of run lengths
0–512 pixels is quantified thus:

representation of digitised image with grey levels (direction of examination 0°→)	matrix (at 0°)			
		run length, i		
		1	2 3 4	
	grey level value, j			
0 1 2 3	0	4 0 0 0		
0 2 3 3	1	1 0 1 0		
2 1 1 1	2	3 0 0 0		
3 0 3 0	3	3 1 0 0		

We are only concerned with a matrix derived from a small portion of the total
foam. Excellent reviews on grey level run length analyses are presented by
Haralick (1979) and Galloway (1975). Having derived the GLRL matrix of the
image it is then possible to extract a number of texture features as follows:

Short Run Emphasis (Galloway 1975). This function divides each run length value by the length of the run squared, consequently the method emphasises the short run lengths which exist in the image. The matrix is normalised by dividing each value by the total number of runs in the image (T_R). A high value relates to a greater number of short runs (i.e. an image with fine 'grainy' structure).

$$SRE(\theta) = \frac{1}{T_R} \cdot \sum_{i=1}^{Ng} \sum_{j=1}^{Nr} \frac{p(i,j)}{j^2} \tag{2}$$

with
$$T_R = \sum_{i=1}^{Ng} \sum_{j=1}^{Nr} p(i,j) \tag{3}$$

Let θ be the angle of examination of the matrix, N_g be the number of grey levels in the picture, N_r be the number of run lengths the $p(i, j)$ be an element of the run length matrix i.e. the number of times there is a run of length j which has a grey level of i.

Long Run Emphasis (Galloway 1975). A function which multiplies each run length value by the length of the run squared. The effect is to emphasise longer run lengths. Again the data is normalised by diving each value by the total number of runs in the image, T_R. A high value of this function relates to more long run lengths contained in the image and may be interpreted as a coarser image.

$$LRE(\theta) = \frac{1}{T_R} \cdot \sum_{i=1}^{Ng} \sum_{j=1}^{Nr} j^2 p(i,j) \tag{4}$$

Grey Level Distribution (Galloway 1975). As the name suggests this function, also known as grey level nonuniformity, indicates the distribution of grey levels in the image. This function squares the number of run lengths for each grey level. The sum of the squares is then divided by the normalising factor T_R. If the frequency of runs is distributed widely the function assumes its lowest values.

$$GLD(\theta) = \frac{1}{T_R} \cdot \sum_{i=1}^{Ng} \left(\sum_{j=1}^{Nr} p(i,j) \right)^2 \tag{5}$$

Run Length Distribution (Galloway 1975). Also referred to as run length nonuniformity. This function squares the number of runs at each run length. The

sum of the squares is then divided by T_R, which has the effect of normalising the values. Where runs are equally distributed throughout a wide range of run lengths the function has a low value. Consequently large run counts contribute most significantly to this function.

$$RLD(\theta) = \frac{1}{T_R} \cdot \sum_{i=1}^{Nr} \left(\sum_{j=1}^{Ng} p(i,j) \right)^2 \tag{6}$$

Run Percentage (Galloway 1975). A function which is the ratio of the total number of runs to the total number of possible runs if all runs had a run length of 1 pixel. The Quantity has its lowest value for pictures with a good deal of linear structure.

$$RP(\theta) = \frac{1}{T_R} \cdot \sum_{i=1}^{Ng} \sum_{j=1}^{Nr} p(i,j) \, / \, P \tag{7}$$

Let P be the number of points in the picture.

Image Treatment. Processing of acquired images was performed on a Pentium PC using programs written in-house in C++ language by the authors. Analytical programs were run through a Bitmap executable file. The 10 variables (5 at 0° and 5 at 90°) from the GLRLM are referred to here as 'texture features' since they chart the mathematical texture of each image.

Normalisation and Principal Component Analysis. The texture features obtained by the GLRL method were gathered in a data matrix, Z for further mathematical treatment. The matrix included 218 rows (corresponding to the 218 acquired images) and 10 columns (texture features). The matrix Z was first normalised i.e. each value was divided by the standard deviation of the corresponding column. This was then followed by principal component analysis (PCA), which was performed on the normalised matrix, taking each row as an observation and each column as a variable.

PCA (Joliffe 1986) provides a means of describing the overall properties of the image, under the highly standardised conditions used the appearance of images is a function of the properties of the foam and solution. In the method we assign a relative distance or spacing to vectored texture features, choosing the simplest distance, which is the Euclidean distance. Thus we find a 'reduced' space by defining limits of the factorial co-ordinates (scores; i.e. scores A1 and A2). The advantage of PCA is in its ability to effectively condense texture features because the technique employs the creation of so-called synthetic variables, referred to as 'components or scores'. These components (scores) are linear com-

binations of the original matrix (post texture analysis) values and not correlated together. The significance of this technique is that it reduces the number of variables to a workable level, and when presented in a visual format in the form of a map, samples with similar attributes appear as near neighbours. The axes or components presented on a PCA map may not be weighted to the same extent. The weighting can be assessed by viewing the eigenvalues for the values corresponding to each axis. This provides a means of assessing the importance of the spatial distribution of sample scores on the plot.

The biplot (map) of the components can be interpreted as a characterisation of the similarity of the 'observations'. Neighbouring points on the biplot represent observations that are similar with respect to some visual characteristics and observations that are relatively far from one another are very different. In the present case, where observations represent the texture features, it was expected that, as the appearance of the foams change relatively slowly during the test, two time-successive images might give similar texture features and consequently would be plotted in close proximity to one another on the graph. Moreover, the scatter distribution of the principal image scores (A1 and A2) for the same series (same parent solution) on a PCA plot was expected to be an indication of the variation of_texture appearances during the test; if the foams were very stable, with respect to bubble morphology, the texture features would not change noticeably and the corresponding points would therefore occupy a small area. The reverse may be true for foams demonstrating much change in morphology.

RESULTS AND DISCUSSION

Foam and Air-water Surface Measurements

In general proteins and low molecular weight emulsifiers, stabilise bubbles in foams by adsorbing at the air-water interface. They stabilise foams by different and totally incompatible mechanisms (Clark 1995). Steric constraints and an elastic-like nature of the protein adsorbed layer prevent close approach of bubbles. The result is that protein-stabilised foams drain much more slowly than ones stabilised by emulsifiers. In addition, over relatively short time periods (minutes or hours) foams that are stabilised by protein retain much more liquid in the foam matrix (Coke *et al.* 1990; Sarker *et al.* 1995a). Consequently, an inherent instability and increased rate of drainage takes place over foams composed of protein alone, when emulsifiers and proteins are combined in the same solution used to generate a foam.

This mechanism of foam instability is a result of the competitive adsorption (Sarker *et al.* 1995a; Courthaudon *et al.* 1991; Clark *et al.* 1993; Dickinson *et al.* 1993) of proteins and emulsifiers at the surface of each bubble in the foam.

The stability of foams is governed chiefly by the physical and rheological pro-
perties of the interface (adsorbed layer). The basis of the different properties of
the adsorbed layer surrounding each bubble in a foam is dictated by the surface
activity and chemical structure of components. Thus, this study involving model
foam systems provides an interesting reference for food foams, which are usual-
ly complex mixtures of proteins and low molecular weight surfactants (polar lipids,
emulsifiers and surfactants).

Foaming studies (Table 2) indicated a significant difference in the evolution
and stability of foams. Foams composed of protein alone or the emulsifier, Tween
20 showed significantly higher initial foam densities (foamability; D_0) than when
the two components were mixed. Thus, in the unmixed foams this relates to smaller
and more numerous bubbles per unit volume of the foam. The values in Table
2 may be a little confusing at first sight, without prior knowledge of the stages
involved in the foam drainage process.

Foams, first drain by a gravitational mechanism, which is essentially indepen-
dent of the bubble size distribution. After a period the interfaces of two adjacent
bubble approach one another so that the interceding foam lamella thickness is
reduced. The liquid drains to a space at the edge of the planar foam lamella, called
the Plateau border. A second mechanism then becomes dominant, known as
capillary drainage. In this mechanism, liquid entrained in the foam lamellae is
under a higher pressure than in the Plateau border and hence moves to the low
pressure border and is thus conveyed out of the body of the foam by gravitational
drainage (Narsimhan and Ruckenstein 1996).

Consequently the stability of foams after 11 min (D_{660}) appears to be very similar
for the casein samples (CA-CC; CAX-CCX), and ovotransferrin samples (OA-
OC; OAX-OCX). The only significant apparent difference was found in the Tween

TABLE 2.
DERIVED QUANTITIES FROM CONDUCTIVITY MEASUREMENTS. DENSITY REFERS TO
THE VOLUME OF LIQUID (mL) ENTRAINED IN THE FOAM DIVIDED BY THE MAXIMUM
VOLUME OF NITROGEN INCORPORATED INTO THE FOAM (mL) AT A CONSTANT FOAM
VOLUME OF 35 mL.

SAMPLES	Initial foam density D_0	Density after 11 minutes D_{660}	Density change ΔD $(D_0-D_{660}/D_0) \times 100$
CA, CB, CC	0.143±0.006	0.053±0.004	61.4
CAX, CBX, CCX	0.119±0.008	0.050±0.004	58.0
OA, OB, OC	0.168±0.002	0.057±0.003	66.1
OAX, OBX, OCX	0.134±0.011	0.055±0.006	59.0
BA, BB, BC	0.124±0.023	0.046±0.008	66.6
TA, TB, TC	0.204±0.011	0.026±0.002	87.3
TAV, TBV, TCV	0.170±0.017	0.023±0.001	86.5

20 samples (TA-TC; TAV-TCV), which showed a much lower foam stability (D_{660}) values. A similarly complex picture was obtained with the density change (ΔD) between initial (D_0) and intermediate (D_{660}) examination. Here, samples containing protein and emulsifier appeared to drain less than foams formed from protein alone. Since the foam took approximately 2 min in each case to form and drainage from the foam is much more rapid in the case of the emulsifier the dynamic adsorption properties become important considerations and are likely to dominate the foam drainage behaviour (Clark *et al*. 1993). In effect, we do not view samples within the same stage of evolution in mixed systems and systems containing only protein, after 2 min of sparging. The data (Table 2) show similar general behaviour with respect to the density change for protein and emulsifier/protein samples. This is a limitation of the conductimetric technique but highlights the need for a more discriminating technique when the foams were visibly different.

However, a significantly different density change was found with Tween 20 alone with low and enhanced viscosity, a difference of approximately 20%. This behaviour agrees well with the reported behaviour of surfactant foams (Narsimhan and Ruckenstein 1996; Germick *et al*. 1994). Such a change was congruous with the observations of the foams containing Tween 20 which changed noticeably from round bubble to polyhedral cell morphology. Little difference was observed in the foam on addition of sucrose (to a final solution concentration of 0.25M) to the Tween 20 solution. The kinematic viscosity was noted to change from almost identical values in the range 1.038–1.047 mm^2s^{-1}, for most samples (1.032 mm^2s^{-1} for the buffer) to 1.202 mm^2s^{-1} for the TAV, TBV and TCV samples. However, this change only undertaken to increase the viscosity of the solution, did appear to reduce the initial foam density, corresponding to larger bubbles in the foam. The viscosity enhancement also increased the time taken for half of the foam liquid to drain from the foam, from 290 to 315 s for Tween 20 foams with sucrose indicating a significant effect on foam drainage in the presence of sucrose. Such a difference corresponds to a greater retention of liquid in the more viscous Tween 20 system but appeared to be only really significant with the conductivity measurements over the first half of the draining process. Since drainage was slowed, the tendency toward bubble coalescence and thus foam appearance would also be changed. This is reasonable, considering that the first part of the drainage of a foam is dominated by gravitational drainage. The underlying assumption in this experiment is that sucrose acts at a neutral agent and can be used to alter the viscosity of the medium. The concentration used is unlikely to have significantly impeded diffusion of Tween 20 to the interface which is usually exceedingly rapid. Such negligible changes, may account for the small differences in bubble sizes between the Tween 20 samples and hence foamability values.It was observed typically, that 65–80% of the liquid in the foam drained from the foam in all samples with the exception of Tween 20 samples, in this case the liquid drained from the foam after a 20 min period was closer to 90+%.

The basis of such differences in foam appearance has its roots in the surface activity of the protein and emulsifier used. The ability of the amphiphile (emulsifier, protein) to diffuse to and adsorb at the air-water interface of a bubble can be quantified by studying the reduction in surface tension produced at a macroscopic air-water interface, when the surface active agent forms an adsorbed layer. The surface tension reduction after 30 min equilibration (γ_{30}) for dilute solutions is presented in Table 3. The data show two significant trends. The first illustrates that the emulsifier Tween 20 adsorbs more readily than the protein samples used and produces the lowest surface tension i.e. is the most surface active. The second, addition of Tween 20 to solutions containing the proteins β-casein and ovotransferrin produced solutions with surface tensions closer to that of Tween 20 alone. This phenomenon of competitive adsorption of surfactant over protein at the interface (Coke *et al.* 1990; Courthaudon *et al.* 1991; Dickinson *et al.* 1993) is now well documented. The magnitude of this displacement of protein from the interface at a molar ratio, $R = 1$ suggested that at equivalent molar concentrations Tween was more effective at displacing ovotransferrin than β-casein from the interface. Despite using different protein concentrations in the foaming and surface tension studies a similar modification of surface properties by Tween 20 might be expected in the more concentrated protein solutions used to form foams.

In another series of experiments, performed at an even lower protein concentration (2 μM), the rate of surface tension reduction was noted to be in the order of Tween 20 > β-casein > BSA > ovotransferrin, with Tween 20 being the most rapid. This explains how Tween 20 appeared to reduce the surface tension of ovotransferrin solutions more than β-casein. In yet another set of experiments but with surface shear rheology, preliminary results indicated that the relative

TABLE 3.
MEASURED QUANTITIES AND OBSERVATIONS FOR MORE DILUTE PROTEIN, EMULSIFIER AND PROTEIN/EMULSIFIER 0.1M SODIUM PHOSPHATE BUFFERED SOLUTIONS FROM SURFACE TENSION MEASUREMENTS AFTER 30 MIN. THE QUANTITY R REFERS TO THE MOLAR RATIO OF EMULSIFIER (TWEEN 20) TO PROTEIN

DILUTED SAMPLES	Dynamic surface tension (γ_{30}) mNm^{-1}	Rate of surface tension reduction for 2μM solutions
Water	72.8	-
10μM β-Casein	49.6	RAPID
10μM β-Casein(+Tween 20), $R=1$	44.2	-
10μM Ovotransferrin	46.8	VERY SLOW
10μM Ovotransferrin(+Tween 20), $R=1$	40.2	-
10μM Bovine serum albumin	53.2	SLOW
10μM Tween 20	39.0	VERY RAPID

surface 'rigidity' (torque of the measuring apparatus at angular velocity of 0.1 rad s^{-1}) of the adsorbed layer, in solutions with the same protein composition as the foaming solutions, was 2, 1.5, 1.3 and 0.1 Nm^{-2} for BSA, β-casein, ovotransferrin and Tween 20, respectively. This provides us with a comparative tool with which to assess to effect of surface rheological properties on bubble morphology. The modelling and calculation of absolute surface shear viscosity values is the subject of our continuing studies. Here, the 'viscoelasticity' or rigidity of the Tween 20 sample adsorbed layer was measured to be of a similar magnitude to that of pure water. However, the relative surface rigidity values are comparable, to some extent with surface dilational modulus (elasticity) measurements (Sarker 1995b) for Tween 20 (1 μM) and BSA (0.3 μM) with values of 20 mNm^{-1} and 60 mNm^{-1}, respectively, that clearly demonstrate significant viscoelastic differences between Tween 20 and BSA stabilised interfaces. In addition, as with the surface tension, and possibly also reflecting the kinetics of diffusion to the interface, the relative surface rigidity of the ovotransferrin interface was extremely slow to develop. Since surface rheological properties are so pivotal to the anticoalescence characteristics of foams (Clark 1995; Clark et al. 1993) the surface tension and rheological properties can be considered integral to the appearance of the initial, intermediate and final images of the foams collected.

Artificial Visual Assessment

Bubble Counting. As a consequence of the difficulty in determination of discriminating physical parameters in foam structure during the drainage process, despite apparent obvious visual differences in bubble size and morphology a series of texture analyses and bubble counting regimes were applied to the foam. Not only was it clear from the images on viewing of the foam itself *in situ* but foam studies are full of references to the structural evolution of protein and emulsifier/surfactant foams with time.

In a simple bubble counting experiment (Fig. 3) the number of bubbles crossing the central axis of the image in horizontal and vertical directions was averaged. The standard deviation of samples was generally of the order of plus or minus one bubble. In general, no significant difference in the number of bubbles in the horizontal and vertical directions was found. Thus, indicating there was no particular bias in any direction. This is possibly related to the positioning of the camera, volume of foam and relatively small area sampled. It was reasonably clear to not only distinguish foam samples by their original 'number' of bubbles but also by the manner in which the number of bubbles changed as a function of time (corresponding to a defined image number). The largest number of bubbles in the initial measurement and therefore in the 5 mm × 5 mm image was found in Tween 20 foams. Tween 20 foams also showed the most rapid bubble
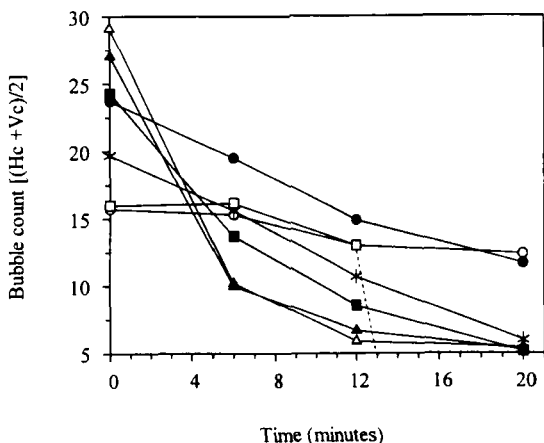
FIG. 3. RESULTS FROM A SIMPLE BUBBLE COUNTING
TECHNIQUE

Plotted on the graph are the average number of bubbles traversed
by intersecting lines in the centre of the image in the horizontal
(Hc) and vertical (Vc) directions (bubble count) against time. The
sample types are represented as follows: CA-CC (○), CAX-CCX
(●), BA-BC (*), OA-OC (□), OAX-OCX (■), TA-TC (△) and
TAV-TCV (▲). The coding used is referred to in Table 1.

growth and also the greatest foam density change, with foams after 6 min (image number 4) drainage assuming the largest bubble size (lowest bubble count value) of all the samples, of 10 bubbles per 5 mm. Addition of sucrose to increase the viscosity (15–16% enhancement over unadjusted samples) of the intralamellar foam liquid only appeared to reduce the initial bubble number and hence increase bubble size. This corresponds closely with the results of foamability measurements. After 6 min drainage (image number 4), Tween 20 foams in the presence and absence of sucrose appeared to be identical, with respect to the bubble count value. β-casein foams (CA-CC) were the most stable with respect to bubble size changes. Initially, ovotransferrin foams also showed a good degree of similarity with β-casein foams but differed in that no images of the foams were collected after 14 min (indicated in the figure by the broken line) because the foam had collapsed either fully or partially below the fixed level of the video camera. The reason for this repeatable observation remains unclear.

Further evidence was also obtained for the competitive adsorption phenomenon at the interface as all protein foams in the presence of Tween 20 showed a similar initial bubble size distribution (Fig. 3) to foams composed of Tween 20 alone. With the ovotransferrin samples both surface tension and the bubble counting technique suggested that in the presence of Tween 20 foams assumed a character

similar to that of foams composed of Tween 20 alone. BSA foams were shown to be generally relatively unstable, in that the initial average bubble count showed a nearly linear decrease in bubble count or linear increase in bubble size with time. It is highly likely that because of the polydispersity of bubble sizes and the rigid-like adsorbed layer the foam instability was a consequence of increased disproportionation rather than bubble coalescence. Ovotransferrin/Tween and β-casein/Tween foams were also relatively unstable. Ultimately, these foams contained approximately the same number of bubbles as the emulsifier foams. This also partially confirms some of the rheological information and surface tension data which suggested that the adsorbed layer of these foams was poorly interacting and dominated by the emulsifier and thus, may have facilitated disproportionation (gas transfer between bubbles of widely varying size) and more significantly bubble coalescence (Clark 1995; Dickinson *et al.* 1993; Narsimhan and Ruckenstein 1996).

One disadvantage with the bubble counting method was that it failed to show samples which were visibly heterogeneous. This is crucial to the understanding of foam behaviour since liquid-based foams always change from exhibiting a more fine structure (e.g. Fig. 4a) to a more coarse structure (e.g. Fig. 4b). Normally, foams which show a polydisperse distribution of bubble sizes and have a highly soluble gas (e.g. carbon dioxide) as the dispersed phase change relatively rapidly under the influences of disproportionation and bubbles with poor surface viscoelasticity change rapidly due to coalescence. In these experiments a minimal aqueous solubility of the nitrogen and a relatively uniform initial bubble size distribution significantly reduced the contribution of disproportionation to the foam destabilisation process. Several foam samples were principally monodispersed after or shortly after formation of the foam, for example β-casein and Tween 20. While, others such as the ovotransferrin/Tween and particularly BSA (Fig. 4c) were exceptionally polydispersed with large standard deviations in the bubble count (e.g. ± 4 bubbles with an average of 20, average values are presented in Fig. 3). A fuller description of the polydispersity of the foam bubble is essential in order to reach a better appreciation of the foam structure. This is pivotal to a more comprehensive understanding of the influence of physico-chemical parameters on foam morphology and its subsequent effect on long-term foam stability.

Texture Analysis. A series of mathematical manipulations were performed on foam images. The aim was to describe both the number of bubbles and morphology of the bubbles present in each of the foam images. Since the principal driving force for the evolution of foams (small bubbles $\rightarrow$ large bubbles) is dictated by the physical characteristics of the solution used to form the foam and the foam itself, an accurate description of the appearance of the foam should go part of the way to amalgamating the full array of physical parameters involved.
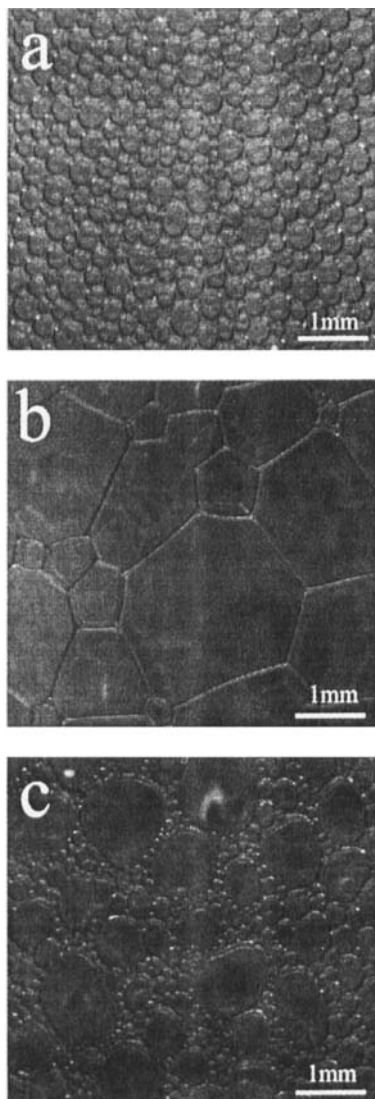
FIG. 4. THREE IMAGES OF PROTEIN
AND EMULSIFIER LIQUID FOAMS AT
VARIOUS STAGES IN THE DRAINAGE
PROCESS
(a) initial β-casein, (b) Tween 20 foam after
20 min drainage and (c) bovine serum albumin
foam after 10 min drainage.

PCA was performed on the matrices produced after texture analysis by the GLRLM technique. The results of the PCA analysis for grey-level run length (GLRL) are presented in Fig. 5. Two components are plotted on the map. Components A1 and A1 represent the most significant 'scores' or factorial coordinates of the texture features ($>$ 97% of total information). Axis A2 (score A2) initially appeared to be related to bubble morphology but on further investigation of individual images appeared to be more closely related to the range of intensities within the image. Under ideal conditions, the range of intensities in the foam images should scale with bubble size and form. This would be useful if the images were entirely regular, however on closer inspection the images contained certain points of reflected light, which varied from sample to sample. For samples with a similar general appearance this component would permit the differentiation of sample foams which would be nearly impossible to distinguish with the naked eye. This could be important but relies on the premise that all samples would scatter to the same extent and does not anticipate microheterogeneity in the sample, leading to much more scattered light in replicates of the same system. In addition, the grey level values were also observed to change with day-to-day sampling of images. A number of environments could interfere with this regularity for example, the daily change in laboratory luminosity and the low frequency fluctuation of the illuminating light source. Under circumstances where the samples were more regular, the axis A2 could in fact reveal information about bubble morphology, since foams composed to smaller bubbles scatter more light and thus appear whiter than foams with a coarse bubble structure (e.g. Fig. 4a and 4b). In this way it would be possible to assign a numerical value to a particular foam structure.

However, the axis A1 (Fig. 5; score A1) did seem to be particularly well correlated (R^2 = 0.65–0.95; average R^2 = 0.85) with time. All samples started at one side of the axis and showed a regular transition with image number to the far extreme of the axis. Importantly, the degree of change in the magnitude of the score A1 seemed to be a function of bubble size and shape. In all cases with each of the 7 sample types (3 proteins, 2 emulsifier conditions and 2 emulsifier/protein mixtures) the parameter A1 reflected a change in shape of the bubbles. A change in the size and shape of bubbles is a step-wise process, directly related to the physical properties of the adsorbed interfacial layer, which in turn governs bubble coalescence and to a lesser extent bubble disproportionation. In our model foam systems use of nitrogen with its lower aqueous solubility should have reduced disproportionation to a low level and thus changes in bubble size were essentially a result of bubble coalescence. Since component A1 represented a score-value for $>$ 75% (% eigenvalue) of the data information contained in the digitised images a change in the magnitude of this parameter is strongly related to difference in the image/texture/structure of the foams. Negative values reflected extremely
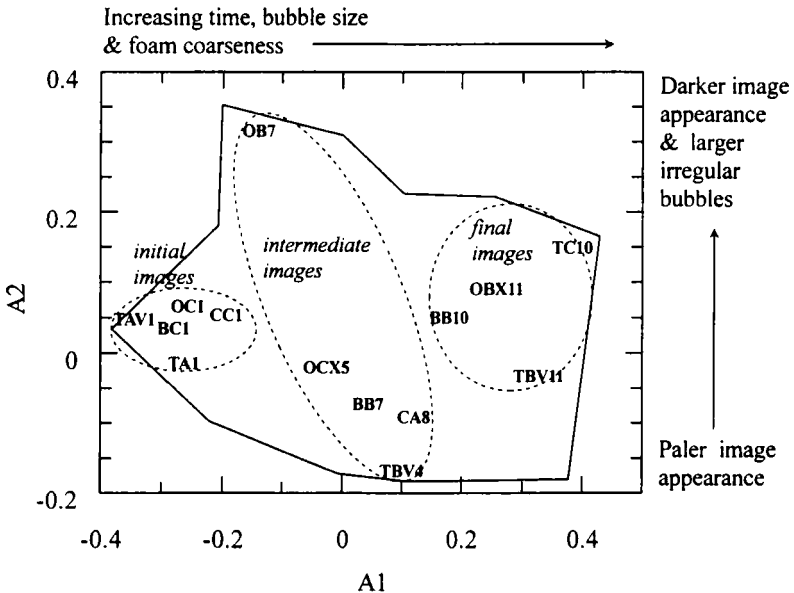
FIG. 5. RESULTS OF PRINCIPAL COMPONENT ANALYSIS (PCA) PERFORMED ON IMAGES TREATED BY THE GREY LEVEL RUN LENGTH MATRIX TECHNIQUE

The values A1 and A2 refer to the major components scores from the analysis. The plot shows the full range of values of components A1 and A2 for the 218 images (bold bordering line). The broken line shows the 'area' occupied by the data points (as sample code) presented. Data points have been omitted for clarity. The coding used is referred to in Table 1, the final digit of the code refers to the sample number in the sequence (at interval of 120 s).

small bubbles of approximately 0.2 mm diameter (e.g. Fig. 4a), whereas values of 0–0.1 corresponded to large rounded polyhedral foams of 0.25–0.5 mm diameters (demonstrated by the larger bubbles in Fig. 4c). Higher values still, corresponded to large angular polyhedral foam cells (e.g. Fig. 4b). The foams contained in this range (Fig. 5) were typically Tween 20 based foams or protein based foams with Tween 20 incorporated into the foam forming solution. Foams containing appreciable concentrations of Tween 20 were well drained after 20 min and were composed of extremely angular polyhedral gas cells reflected in the highest value of the component A1 observed of 0.3–0.4. This is the domain where conductivity measurements are least valuable because the technique cannot differentiate between different bubble forms to the same extent. This parameter A1 is a valuable tool with which to delineate bubble size and shape changes in model foam systems.

The series of data curves shown in Fig. 6, illustrate the time based evolution (left to right) of the foams for 4 major categories of samples, these are β-casein,
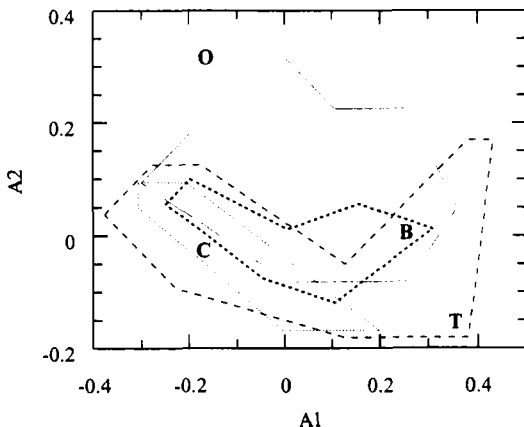
FIG. 6. DETAILED 'FOCUSED' REPRESENTATION OF
DATA FROM FIG. 5. PRINCIPAL COMPONENT ANALY-
SIS DATA FOR THE FOUR MAIN GROUPS OF AIR-
WATER FOAMS
Samples were: β-casein foams in the presence and absence of
Tween 20 (C; fine broken line), ovotransferrin foams in the
presence and absence of Tween 20 (O; solid line), bovine serum
albumin foams (B; broken line) and Tween 20 foams in the
presence and absence of sucrose (T; coarse broken line), to
enhance the bulk viscosity. Data points have been omitted for
clarity.

ovotransferrin, BSA and Tween 20 foams. The figure shows a 2-D separation
which reveals a 'true' and yet 'mathematically' created separation of images based
on size, shape and intensity. An interesting feature of the biplot lies in its ability
to show such spatial separation of samples. The plots show the principal separa-
tions of coarseness manifested in the parameter score A1. The range of A1 values
covered by the four main classes of amphiphiles appears as follows: β-casein (C)
< BSA (B) < ovotransferrin (O) < Tween 20 (T). This confirms data from
the bubble counting and conductimetric techniques where pure β-casein foam bub-
ble size distributions did not change appreciably during the course of the experi-
ment and Tween 20 foams changed the most.

It is interesting to draw comparisons between two major classes of proteins
used. β-casein (small — 24 kD and poorly surface interacting) and BSA (large
— 67 kD and strongly surface interacting) provide one such example, both oc-
cupy small areas on the biplot but demonstrate that surface rigidity and rheological
properties are not the only important considerations, apparently rapid molecular
diffusion to the interface is important and that is much more rapid for small pro-
tein (and surfactant) molecules. With BSA and ovotransferrin (76 kD), which
are similar in size (molecular weight) but possess different surface/rheological

properties it is noteworthy that the 'area' of A1 and A2 scores occupied by the poorer surface interacting and slowest molecule to diffuse to the surface (Table 3, speed of surface tension reduction), that of ovotransferrin was larger than BSA and produced protein foams which were extremely unstable.

What is confusing in the biplot is the absolute significance of the A2 values since in some instances, for example, β-casein and BSA the range of A2 values was small. However, with visibly coarser ovotransferrin and Tween 20 foams after a period of drainage the range of A2 values was large. Validation of the influences on the component A2 is the subject of our continuing studies. This parameter partially reflects bubble size distribution through scattered light intensity variation. Unfortunately the degree of discrimination on a daily basis is not congruous with that of parameter A1. The significance weighted value of A1 scores was 5 times that of A2 scores. Thus, the unpredictability and lack of consistency of the A2 data negated its use as an analytical tool.

As a consequence of the clear relationship between time and the parameter A1 (Fig. 5) a series of averaged plots were produced that are presented in Fig. 7.
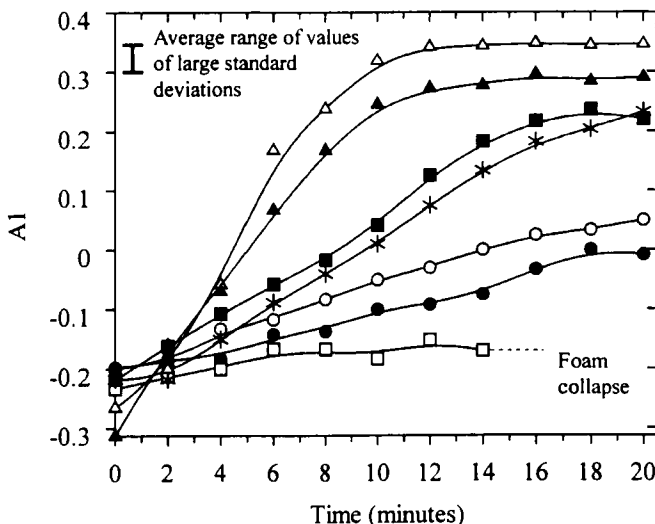
FIG. 7. COMPONENT SCORE A1 FROM PCA OF GREY LEVEL RUN LENGTH TREATED IMAGES OF AIR-WATER FOAMS PLOTTED AGAINST TIME (CORRESPONDING TO IMAGE NUMBER)

Images were acquired every 2 min after the initial acquisition at the end of foam generation. The plots represent β-casein foams in the presence (CAX-CCX; ●) and absence (CA-CC; ○) of Tween 20, ovotransferrin foams in the presence (OAX-OCX; ■) and absence (OA-OC; □) of Tween 20, bovine serum albumin (BA-BC; *) foams and Tween 20 foams in the presence (TAV-TCV; ▲) and absence (TA-TC; △) of sucrose, to enhance the bulk viscosity. The averaged data values are presented in the plots. The coding used is referred to in Table 1.

The initial parts of all plots presented show an initial linear increase in the value of A1 as a function of time. Modelling of the curves is possible but not ideal given that the curves are not fully linear and possibly with the protein and protein/emulsifier systems show a large reduction in the rate of increase at drainage times close to 18–20 min. This is not surprising given the fact that any technique that models foam drainage and evolution should mirror these phenomena, where change is rapid at first but then slows significantly. It seems highly likely that the parameter A1 simply reflects these changes in bubble size/morphology. Each curve does in fact represent the behaviour of the foam very well but comparisons on a large-scale between the radically different samples examined here necessitates a degree of caution.

Several notable features are evident in Fig. 7. Firstly, the parameter A1 essentially represents bubble coarseness throughout the foam and more specifically the foam image. The greatest change in the samples was seen with Tween 20 foams. Tween 20 foams also showed the greatest change in foam density during the 20 min of the experiments. The value of the PCA component in this instance is not only significant in the range of A1 values covered but also in the form of the image related 'drainage' curve. After a period of 10 min the rate of change in morphological texture within the image changed considerably. In principle it should be possible to analyse the gradient of such plots, which simply represent the evolution of the foam as a function of time. The magnitude of such a slope would be a characteristic of the rate of change within the foam (Table 4), with a sharper gradient relating to a more rapid change in bubble size. However, the sample plots show clear differences in form, which clearly correspond to the nature of the amphiphile used to stabilise the foam. One notable feature of the plots is that all protein and protein/emulsifier samples showed a nearly linear change in the magnitude of the parameter A1 with time. In contrast the Tween 20, sample curves (TA-TC; TAV-TCV) showed a dual character. Over the time period 0–10 min (images 1–6) all Tween 20 samples showed a sharp increase in the value of the score A1, but after this period the plots showed small but significant reductions in the rate of change, corresponding to a saturation of changing bubble morphology. Surfactant and emulsifier foams are known to drain to equilibrium foam film thicknesses much more rapidly than protein based foams because they have weaker electrostatic and steric repulsion properties between foam bubbles (lamellae). Since the character of a range of foams was observed it is possible to assign values of the score A1 to specific approximations of bubble forms. It is also possible to measure the initial gradient (relating to rate of change in bubble size/shape) and intercept (lower values relating to smaller initial bubble size) of the curves (Table 4), in this way we are able to characterise foam form, given an appropriate model foam system. The significant change in the slope of the curve (TA-TC) at the 10 min point corresponded to a large reduction in the rate

TABLE 4.
LINEAR REGRESSION OF SCORE A1 PLOTTED AGAINST TIME (0–10 MIN PERIOD) FOR
THE DATA PRESENTED IN FIG. 6

Data represented	Gradient	Intercept	Correlation coefficient (R^2)
β-casein	0.015	-0.21	0.97
β-casein + Tween 20	0.010	-0.21	0.93
Ovotransferrin	0.008	-0.23	0.89
Ovotransferrin + Tween 20	0.026	-0.22	1.00
Bovine serum albumin	0.025	-0.24	0.97
Tween 20	0.064	-0.28	0.97
Tween 20 - enhanced bulk viscosity	0.056	-0.29	0.99

of change within the image textures and to a significant slowing of foam drainage. This is another reason for the limitation of a slope defining characteristic since it depends on the time range over which the slope is measured. Only several of the data curves approximated to a linear form between 0 and 20 min. With the Tween 20 images it is clear that the A1 score charted many sizes and bubble shapes in the image texture. The second observation is that as with the bubble counting method GLRLM method also suggested that the increase in coarseness of the BSA foam images was rapid and nearly linear over the entire time period evaluated. A representation of the findings of the simple but useful bubble counting technique was expressed in the A1 score data when plotted against time.

Finally, the data in Fig. 7 (curves CA-CC, CAX-CCX; OA-OC, OAX-OCX; BA-BC) also highlight differences in the physico-chemical composition of the intralamellar liquid and interfacial adsorbed layer. Surfactants and emulsifiers are known to compete at the interface with adsorbing protein. The net effect is an inherently unstable system in which neither type of molecule dominates (Clark 1995; Courthaudon et al. 1991; Clark et al. 1993). The resulting reduction in viscoelasticity of the interfacial layer leads to more rapid foam drainage and rate of bubble coalescence. In Fig. 7 (curves CA-CC, CAX-CCX; OA-OC, OAX-OCX), the apparent change in texture of the foams formed from β-casein and ovotransferrin, respectively, is relatively slow with shallow gradients. In the presence of the emulsifier, Tween 20 the slope of the change in image texture (score A1) as a function of time was not significantly affected with β-casein samples but changed on a much larger scale in the ovotransferrin foams. Domination of the adsorbed layer by Tween 20 explains why the foams formed from ovotransferrin/Tween 20 mixtures had much smaller bubble sizes than with ovotransferrin alone (Fig. 3). Comparison of the data in Fig. 7 (curves CA-CC, CAX-CCX; OA-OC, OAX-OCX) goes part of the way to describing, pictorially, the degree of influence Tween 20 had on the ovotransferrin and β-casein foam interfaces.

Since the Tween 20 foam system was known to encompass a range of particular textures, proximity to the corresponding A1 value in other samples at a specific time, could be used to identify and indicate the relative composition of the adsorbed interfacial layer.

One major advantage of the score A1 is that it embodied a number of texture features. Statistical analysis of the contributions of the GLRLM parameter to the A1 score showed that the value was positively and strongly correlated with short run lengths (Eq. 2) and long run lengths (Eq. 4) at 0 and 90°, strongly and negatively correlated with run length distribution (Eq. 5). This is to say, that the score A1 was probing the texture for fine and coarse structure but was not correlated with the nonuniformity and was negatively correlated with linearity and GLRL distributions. The fact that the run length distribution values were negatively correlated shows that run lengths were actually relatively randomly distributed throughout the textures. Consequently, it is hardly surprising that the component A1 correlated so well with the time related coarsening of liquid foams.

Although the results showed so many positive qualities, there were also some negative findings in the GLRL study. Primarily, the sensitivity of the technique to minor differences in the luminosity of the measuring environment. To an extent it is also possible that the bubble shapes and rate of coalescence of bubbles was influenced by the nonequilibrium conditions in which the measurements were performed. Conditions such as evaporative losses from the foams, thermal fluctuations in the temperature of the foam, vibrational perturbation of foam bubbles, location of smaller bubbles at the vessel wall and also possible distortion of the image by the vessel wall, however, given that the same equipment was used for acquisition of all images, these problems lose importance as the same degree of bias was present in all cases. In addition, foam formation, stabilisation and drainage are such complicated processes and it is difficult to create ideal study conditions, however this technique proved extremely descriptive and revealing. As to the interference in textures from scattered light, under exceptionally constant lighting conditions this could also prove to be of use in describing liquid foam texture by the GLRL technique since scattered light within a foam is also related to the bubble size distribution. One major advantage with textural analysis of 3-D foams is that although there may be some bias toward smaller bubbles locating at the window of the vessel, to fulfil the geometry of the curved surface, the image texture actually shows a succession of foam lamellae behind the primary layer, closest to the vessel wall. Effectively the 3-D image is compressed and weighted (e.g. Fig. 4b) with reference to its proximity to the camera, to 2-dimensions.

Removal of the interference inherent in our measuring system and use of less dynamic foam samples is the subject of continuing studies. Using standardised samples and conditions we have been able to evaluate both the image analysis

technique and make comparisons with absolute physical measurements. The GLRL model seems ideally suited for describing the distribution and evolution of air-water protein and surfactant foams.

CONCLUSIONS

The complementary approach of textural analysis of foam images proved advantageous over use of more conventional physical measurements (e.g. conductimetry, drainage), which describe some foam properties but not appearance. A more comprehensive description of bubble appearance is essential for a fuller understanding of foam instability. Use of the natural 'intensity weighted' 2-D images allowed description of the relative distribution, size and shape of bubbles in the foam. The advantage in this approach over conventional techniques is that it utilised more than one descriptive parameter (texture feature) in the final component (score) used. In other words no information is lost but rather it is compressed. Conventional methods for example, conductimetry describe liquid retention in the foam but do not provide a sufficient description of the morphology of bubbles. Location of smaller bubbles at the vessel wall introduces a degree of bias in to the measurement but is present to an equal extent in all measurements and does not hinder foam or sample differentiation with time. Bubble form is related to adsorbed layer composition and thus provides a means of evaluating coalescence phenomena.

Absolute measurement of coalescence throughout the measuring process remains difficult to define as bubble coalescence changes the bubble size and can consequently provide a route for continuing disproportionation. However, use of nitrogen as the dispersed phase biased the apparatus toward measurement of coalescence. Being able to predict the likelihood of bubble coalescence allows measurement of long-term stability. The data from textural analyses of images showed a high degree of compatibility with results from a bubble enumeration technique and foam density (conductivity) measurements. The physico-chemical basis for the proliferation of different foam textures helped explain differences in the PCA data. PCA score A1 provided an additional means of identifying adsorbed layer structure and composition. The influence of the surface activity of the amphiphiles (proteins and surfactant) used and bulk viscosity effects have been delineated.

Future studies involving extremely constant lighting conditions may explain the significance of the score A2 and resolve problems with random variations in the luminosity of images. In the present study this component was found to be considerably less significant than component A1. Textural analysis also proved useful in validating the importance and reliability of conductimetric measurements.

The simplicity, nonperturbative nature, descriptive potential and enumeration of relative differences between images of real foams provides a means of assessing the differences in foam structure that relate to adsorbed layer properties. This technique has a strong potential for use in quality control and on-line measurement applications.

ACKNOWLEDGMENTS

NOMENCLATURE AND ABBREVIATIONS

A1: principal component analysis score/factorial coordinate/component 1
A2: principal component analysis score/factorial coordinate/component 2
Biplot: map of principal component scores A1 and A2
Competitive adsorption: interfacial displacement of less surface active molecule (e.g. protein) by more surface active molecule (e.g. low molecular weight surfactant)
Foamability: foam density immediately after cessation of sparging
Foam stability: foam density 11 min after commencement of foaming
GLRL: grey level run length
GLRLM: grey level run length matrix(ces)
PCA: principal component analysis
R: molar ratio of surfactant to protein in solution used to form foams
Texture feature: one of 10 parameters determined from the grey level run length matrix
Tween 20: low molecular weight (1.2 kD) food emulsifier/surfactant

REFERENCES

BERTRAND, D., LE GUERNEVÉ, C., MARION, D., DEVAUX, M.F. and ROBERT, P. 1992. Description of the textural appearance of bread crumb by video image analysis. Cereal Chem. *69*, 257–261.
BERTRAND, D., ROBERT, P., MELCION, J.P. and SIRE, A. 1991. Characterisation of powders by video image analysis. Powder Technol. *66*, 171–176.

CHU, A., SEHGAL, C.M. and GREENLEAF, J.F. 1990. Use of gray value distribution of run lengths for texture analysis. Pattern Recognition Letters *11*, 415–420.

CLARK, D.C. 1995. *Characterisation of Food: Emerging Methods* (G. Gaonkar, ed.) Elsevier Applied Science, London.

CLARK, D.C., WILDE, P.J., BERGINK-MARTENS, D.J.M., KOKELAAR, A.J.J. and PRINS, A. 1993. *Food Colloids and Polymers: Stability and Mechanical Properties*, RSC Special Publication No. 113. (E. Dickinson and P. Walstra, ed.) Royal Society of Chemistry, Cambridge.

COKE, M., WILDE, P.J., RUSSELL, E.J. and CLARK, D.C. 1990. The influence of surface composition and molecular diffusion on the stability of foams formed from protein/surfactant mixtures. J. Colloid Interface Sci. *138*, 489–504.

CONNERS, R.W. 1980. A theoretical comparison of texture algorithms. IEEE Trans. Pattern Anal. Machine Intelligence *3*, 204–222.

COURTHAUDON, J.-L., DICKINSON, E., MATSUMURA, Y. and CLARK, D.C. 1991. Competitive adsorption of β-lactoglobulin + Tween 20 at the oil-water interface. Colloids Surfaces *56*, 293–300.

DICKINSON, E., OWUSU, R.K., TAN, S. and WILLIAMS, A. 1993. Oil-soluble Surfactants have little effect on competitive adsorption of α-lactalbumin and β-lactoglobulin. J. Food Sci. *58*, 295–298.

DICKINSON, E. and STAINSBY, G. 1982. *Colloids in Food*. Elsevier Applied Science, London.

FAINS, A., BERTRAND, D., BANIEL, A. and POPINEAU, Y. 1997. Stability and texture of protein foams: A study by video image analysis. Food Hydrocolloids *11*, 63–69.

GALLOWAY, M.M. 1975. Texture analysis using gray level run lengths. Computer Graphics and Image Proc. *4*, 172–179.

GERMICK, R.J., REHILL, A.S. and NARSIMHAN, G. 1994. Experimental investigation of static drainage of protein stabilized foams — comparison with model. J. Food Eng. *23*, 555–578.

GUILLERME, C., LOISEL, W., BERTRAND, D. and POPINEAU, Y. 1993. Study of foam stability by video image analysis: Relationship with the quantity of liquid in the foams. J. Texture Studies *24*, 287–302.

HARALICK, R.M. 1979. Statistical and structural approaches to texture. Proceedings IEEE, *67*, 786–804.

JOLIFFE, I.T. 1986. *Principal Component Analysis*. Springer Series in Statistics, New York.

KRÄGEL, J., SIEGEL, S., MILLER, R., BORN, M. and SCHANO, K.-H. 1994. Measurement of interfacial shear rheological properties: An automated apparatus. Colloids Surfaces A: Phys. Eng. Aspects *91*, 169–180.

LOHMANN, G. 1995. Analysis and synthesis of textures: A co-occurence based approach. Comput. & Graphics *19*, 29–36.

LOISEL, W., GUÉGUEN, J. and POPINEAU, Y. 1993. *Food Proteins Structure and Functionality* (K.D. Schwenke and R. Mothes, eds.) VCH Publishers, New York.

NARSIMHAN, G. and RUCKENSTEIN, E. 1996. *Foams. Theory, Measurements and Applications*, Surfactant Science Series 57 (R.K. Prud'homme, S.A. Khan, eds.) Marcel Dekker, New York.

SARKER, D.K., WILDE, P.J. and CLARK, D.C. 1995a. Competitive adsorption of L-α-lysophosphatidylcholine/β-lactoglobulin mixtures at the interfaces of foams and foam lamellae. Colloids Surfaces B: Biointerfaces *3*, 349–356.

SARKER, D.K. 1995b. *Control of Protein Foam Stability by Crosslinking*, Ph.D. Thesis, The University of East Anglia, England.